Broadband parasitic modeling of diodes in the millimeter-wave band

Mario Pérez-Escribano, Angel Palomares-Caballero, Pablo Padilla, Juan F. Valenzuela-Valdes, Enrique Márquez-Segura

Int. J. Electron. Commun. (AEÜ) 177 (2024) 155216

Contents lists available at ScienceDirect

Int. J. Electron. Commun. (AEÜ)

journal homepage: www.elsevier.com/locate/aeue

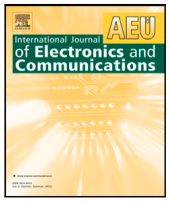

Short communication

Broadband parasitic modeling of diodes in the millimeter-wave band

Mario Pérez-Escribano [a,c,*], Ángel Palomares-Caballero [b], Pablo Padilla [c], Juan F. Valenzuela-Valdés [c], Enrique Márquez-Segura [a]

[a] Telecommunication Research Institute (TELMA), Universidad de Málaga, E.T.S. Ingeniería de Telecomunicación, Boulevard Louis Pasteur, 35, Málaga, 29010, Málaga, Spain

[b] Institut d'Électronique et des Technologies du numéRique (IETR), National Institute of Applied Sciences (INSA) Rennes, UMR CNRS 6164, Rennes, 35708, France

[c] Department of Signal Theory, Telematics and Communications, Centre for Information and Communication Technologies (CITIC-UGR), University of Granada, Calle Periodista Rafael Gómez Montero, 2, Granada, 18071, Spain

ARTICLE INFO

Keywords:
Broadband characterization
Equivalent circuit
Millimeter waves
Parasitic modeling
PIN diode
Varactor

ABSTRACT

This paper presents the extraction of an equivalent circuit model for PIN diodes and varactors in the millimeter waves. This circuit model is handy for new communication applications involving, for example, electronic beam reconfigurability, where diodes are commonly used. For parameter extraction, the proposed model includes the effects of the device, the pads, and the gap underneath the device. From the measurement at various bias points (varactor) or states (PIN diode), it is possible to extract an equivalent circuit to properly model the behavior of these devices when using them to design reconfigurable elements. The results are validated experimentally, obtaining an excellent agreement between the measurements and the equivalent circuit models in a large frequency band up to 67 GHz.

1. Introduction

In the context of upcoming communication systems, there will be a rise in their operating frequencies to circumvent the congested sub-6 GHz spectrum and obtain greater bandwidth. The proposed frequency range for future communications devices is in the millimeter-wave frequency band (30–300 GHz) [1]. Nonetheless, this frequency range poses an engineering hurdle as it leads to a remarkable increase in the propagation losses of the wireless links [2]. To overcome this issue efficiently, the radiating systems should increase their gain and have the ability to reconfigure the direction of their main beam [3]. Therefore, the integration of reconfigurability mechanisms for the radiation pattern is strongly required in the next generation of radiating devices.

Several strategies have been proposed in the literature to give reconfigurability to radiation patterns, among which the use of diodes is one of the most widely adopted [4,5]. Specifically, most studies that use diodes in their antenna designs do so for frequencies in the sub-6 GHz band [6–10]. The main reason for not using diodes for higher frequencies is their size since parasitics start appearing and becoming significant for their electromagnetic performance [11]. This undesired parasitic effects in diodes is due to how the diode is manufactured and the packaging used for its integration and soldering. Generally, in research works reporting antenna designs with diodes for frequencies below 6 GHz, the diodes have surface-mount device (SMD) packaging. However, as the operating frequency increases for diodes with this type of packaging, parasitic effects must be considered to predict their behavior and produce an accurate design [12]. In addition, parasitic effects also depend on the device assembly.

Another type of device packaging, named flip chip packaging, provides a broader frequency operating range. PIN diodes with this type of packaging have been selected for prototypes above 10 GHz [13–18]. With this packaging, the parasitic effects are mitigated, and the circuit model of the diode is extended in frequency to use it in the design process. The previous research works use a PIN diode that allows the adoption of two states depending on the diode bias. There is also another type of diode called varactor that, depending on the bias voltage, allows a continuous variation of the value of a variable capacitance located in its circuit model. Using this type of diode is beneficial in antenna design since, for example, it allows a gradient in phase for the radiating elements to be obtained. For this type of diode, a commercial flip-chip packaged model has been used in several antenna designs reported in the literature such as leaky-wave antennas [19,20], phased arrays [21], transmitarrays [22] and, reflectarrays [23].

* Corresponding author at: Telecommunication Research Institute (TELMA), Universidad de Málaga, E.T.S. Ingeniería de Telecomunicación, Boulevard Louis Pasteur, 35, Málaga, 29010, Málaga, Spain.

E-mail addresses: mpe@ic.uma.es (M. Pérez-Escribano), Angel.Palomares-Caballero2@insa-rennes.fr (Á. Palomares-Caballero), pablopadilla@ugr.es (P. Padilla), juanvalenzuela@ugr.es (J.F. Valenzuela-Valdés), ems@ic.uma.es (E. Márquez-Segura).

https://doi.org/10.1016/j.aeue.2024.155216
Received 10 January 2024; Accepted 27 February 2024
Available online 6 March 2024

The datasheets of the diodes mentioned in the previous research works usually include information about some of their circuit parameters depending on their bias. Unfortunately, the circuit values given are for certain frequencies or are incomplete. In addition, these datasheets do not usually include the maximum operating frequency of the diode, after which its performance starts to deteriorate due to the appearance of parasitic effects. In order to bring light to this general issue found in most PIN diode and varactor datasheets, this paper presents a broadband RF modeling of these devices up to 67 GHz. This characterization fills the gap about the unknown performance of commercial diodes at millimeter-wave frequencies. In other words, it allows us to know the circuit values that model the behavior of commercial PIN and varactor diodes at this frequency range. This characterization predicts the electromagnetic performance of reconfigurable RF devices (such as antenna arrays) more accurately for this frequency range. It is important to remark that the maximum operating frequency found in all the above research works about reconfigurable antennas was around 30 GHz. The broadband modeling has been performed on two of the most commonly used diodes (PIN [24] and varactor [25]) for RF designs above 10 GHz. These diodes have flip-chip packaging suitable for millimeter-wave frequencies. In this paper, we will present the broadband characterization and the equivalent circuits used to model the performance of the diodes, their comparison with the circuit models used so far, and the limitations of these diodes in the studied frequency range (up to 67 GHz).

2. Equivalent circuit extraction

2.1. Measurement setup

The diodes chosen to be characterized in this work are MACOM PIN diode MA4AGP907 and varactor MAVR-011020-1411. To properly characterize the electromagnetic response of both diodes, it was decided to use a microstrip transmission line due to its low manufacturing cost, the possibility to cover the whole bandwidth of the vector network analyzer (VNA), and the ease of soldering the diodes onto the line. For this purpose, a through-reflect-line (TRL) calibration kit was designed and manufactured over Rogers RO4003C substrate, 20 mils of thickness, and $\varepsilon_r = 3.55$. The line width is 1.22 mm for a 50 Ω characteristic impedance. The gap left for attaching the PIN diode measures 350 μm, whereas the one for the varactor is 228 μm long. The complete equivalent circuit presented in Fig. 1(a) will comprise four blocks. Three will depend on the chip and how it is soldered, whereas the last one will vary with the transmission line and gap size. A photograph of the manufactured setup, including the welded diodes, is shown in Fig. 2. Measurements are taken with a Keysight PNA-X N5247B, from 1 to 67 GHz, using −5 dBm in each port. The PNA-X employs internal bias tees on each port to bias the diodes.

2.2. Gap and pad modeling

As shown in Fig. 1, the model comprises four clearly differentiated blocks. The first and third blocks, highlighted in orange, represent the pads. The connecting pads can be effectively modeled as a π-network [26,27], encompassing both pad capacitance and pad inductance values. This π-network depiction adequately captures the pad behavior when the pad length is below 10% of the effective wavelength at the highest frequency, and its characteristic impedance remains dispersion-free. The second block, highlighted in purple, encompasses the intrinsic effects of the device and will be studied in depth in Section 3.

The fourth block, highlighted in yellow, corresponds to the gap where the varactor is placed. This gap can be modeled as a capacitor, including capacitive effects, connected in parallel with a conductance that will consider the radiation effects [28] and will vary with frequency. The capacitors C_{gap} obtained are 28.5 fF for the varactor and

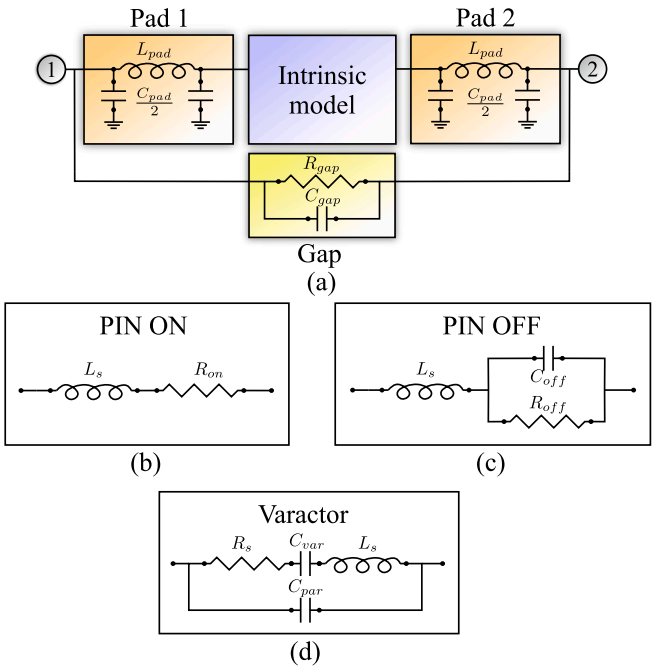

Fig. 1. Equivalent circuit of the (a) complete measurement scheme, including pad and gap effects, (b) intrinsic PIN diode (ON state), (c) intrinsic PIN diode (OFF state), (d) intrinsic varactor. (For interpretation of the references to colour in this figure legend, the reader is referred to the web version of this article.)

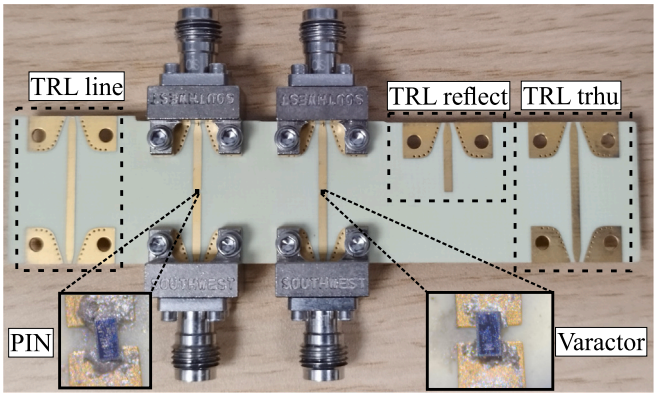

Fig. 2. Photograph of the manufactured measurement setup, including TRL calibration kit and welded PIN diode and varactor.

15.4 fF for the PIN diode, whereas the radiation resistance, R_{gap}, can be calculated as

$$R_{gap} \simeq \frac{1}{\frac{2\pi\sqrt{\varepsilon_{r,eff}}^3}{3\eta_0}\left(\frac{w}{\lambda_0}\right)^2}, \quad (1)$$

being $\varepsilon_{r,eff}$ the effective relative permittivity of the microstrip line, w the width, η_0 the free space impedance, and λ_0 the free space wavelength.

2.3. Fitting process

Once the calibration of the VNA has been performed, the S-parameters, including the effects of the diodes, are measured. However, these parameters are typically influenced by noise and measurement errors. For this reason, to have a better starting point for extracting the equivalent circuit of the diodes, a fitting of the S-parameters is performed to approximate the response properly. Concretely, a rational

fitting of the S-parameters [29] is carried out. It consists of finding a rational function

$$F(s) = \sum_{k=1}^{N} \frac{C_k}{s - A_k} + D, \tag{2}$$

being N, the number of poles considered for the approximation. This technique has proven to be quite efficient in controlling responses with certain errors or resonant peaks to be eliminated [29].

The optimization procedure consists of first fitting the measured S-parameters of the diodes, and subsequently, the processing is carried out in MATLAB®. To obtain the equivalent circuit model, the optimization starts at low frequencies to avoid the parasitic effects of the pads. This way, we assume that the inductors and pad effects are negligible. Once these values are obtained, we move up to high frequencies to find optimal values of the rest of the elements. For this purpose, we minimize the error function

$$\min_{p} \sum_{i=1}^{2} \sum_{j=1}^{2} \frac{1}{2} \left| S_{fit_{i,j}} - S_{eq.circuit_{i,j}} \right|^2, \tag{3}$$

where S_{fit} are the fitted from measured S-parameters, $S_{eq.circuit}$ the ones obtained from the equivalent circuit that is optimized as a function of the elements in the circuit, and p the circuit elements to be estimated.

3. Experimental validation

3.1. PIN diode

The PIN diode is modeled in two states, commonly named "ON" and "OFF". As mentioned previously, the equivalent circuit given in the datasheet of the devices will be the initial guess for the parameter considered to be fitted. We will use 15 mA forward current for the ON state and 0 V for the OFF state, as there is no variation of the behavior with different reverse bias voltages. The procedure starts with the ON state, as the number of parameters to be optimized is reduced. Subsequently, having fixed L_s, the values of C_{off} and R_{off} are computed. The results are summarized in Table 1. The magnitude of the equivalent circuit S-parameters is represented in Fig. 3. As seen, there is an excellent agreement between measured results and those from the achieved equivalent circuit for both states. The values obtained for the intrinsic parameters of the PIN diode are pretty different from those used in other packaging technologies, such as SMD, for reconfigurable antennas up to 6 GHz. In this sense, the commercial PIN diodes Skyworks SMP1345079LF (L_s = 0.7 nH, C_{off} = 0.17 pF, R_{on} = 1.5 Ω, R_{off} = 1 MΩ) [6] NXP BAP65-02 (L_s = 0.6 nH, C_{off} = 0.5 pF, R_{on} = 1 Ω, R_{off} = 20 kΩ) [8], or Infineon BAR50-02V (L_s = 0.6 nH, C_{off} = 0.15 pF, R_{on} = 4.5 Ω, R_{off} = 5 kΩ) [9,10] show a difference in their equivalent circuit of an order of magnitude in series inductance (L_s) or parallel capacitance (C_{off}), which will clearly limit their use in the millimeter-wave band.

3.2. Varactor

To model the varactor, we start from the model given in the datasheet, composed of a series resistance (R_s), inductor (L_s), and capacitor (C_{var}), and connected in parallel with an extra capacitor (C_{par}), to model the parasitic effects of the varactor packaging. It is specified by manufacturer that R_s and C_{var} should vary with the bias voltage. However, there is no information about the possible values of the elements in the equivalent circuit, nor how they change with the bias voltage. The process is carried out in two stages. The initial one considers 0 V bias voltage. The achieved results are summarized in Table 1.

In the second stage, it is necessary to study how the capacitance C_{var} and resistance R_s vary when the bias voltage changes. The equivalent circuit created will now be used as a starting point. Subsequently, the S-parameter response is measured from 0 V to 20 V reverse voltage

Table 1
Extracted PIN diode and varactor parasitic model parameters.

PIN diode			Varactor		
Element	Value	Unit	Element	Value	Unit
L_s	30.3	pH	R_{s0V}	10.2	Ω
R_{on}	4.2	Ω	L_s	88.5	pH
C_{off}	41.3	fF	C_{var0V}	234	fF
R_{off}	100	kΩ	C_{par}	9	fF
L_{pad}	120.2	pH	L_{pad}	42.8	pH
C_{pad}	13.4	fF	C_{pad}	11.7	fF
			V_j	1.8	V
			M	0.75	–

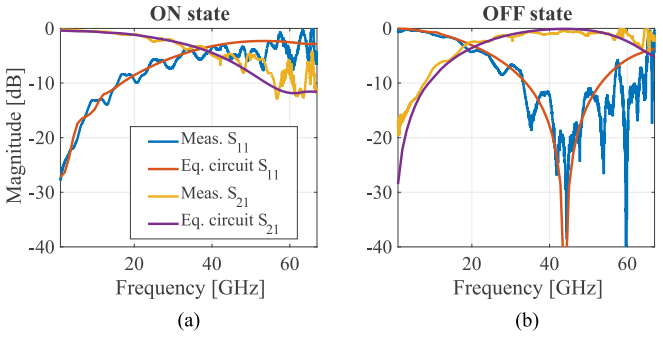

Fig. 3. Measured and equivalent circuit S-parameters of the PIN diode, using (a) 15 mA forward current and (b) 0 V bias voltage.

in steps of 2 V. These data are used to find the optimum capacitance values, following the equation

$$C_{var} = C_{var0V} \left(1 + \frac{V_{dc}}{V_j}\right)^{-M}, \tag{4}$$

being C_{var} the capacity obtained using a reverse bias voltage V_{dc}. From (4), V_j and M are obtained directly. Their values are also indicated in Table 1. Regarding R_s, we proceed similarly. In this case, in the absence of any specific model for the variation of the resistance, what has been done is to sample the value at various bias points and then proceed with a polynomial fit. It has been found that the equation gives the values that make the equivalent circuit fit best

$$R_s(V) = 0.016V_{dc}^2 + 0.07V_{dc} + 10.2. \tag{5}$$

Once this variation has been calculated, the complete equivalent circuit of the varactor can be obtained. Fig. 5 shows the results of the magnitude of S-parameters for 0 V, 6 V, 10 V, and 20 V. As can be seen, there is an excellent agreement between measured S-parameters and equivalent circuits. The variation of C_{var} and R_s with bias voltage is represented in Fig. 4 for V_{dc} = 0...20 V.

To conclude the study, we studied how the response varies according to the position of the diode. For this purpose, the varactor was selected to be soldered in three different positions: upwards (top position), sideways (side position), and backward (bottom position). A photograph of the attached varactor can be seen in the insets of Fig. 6. To model the variation produced by position, different L_{pad} have been used, following the same procedure in the previous section. The values obtained are 42.8 pF (top), 71.3 pF (side), and 100.2 pF (bottom), respectively. As seen, the value of the pad inductance increases when the length of the welding is longer, which physically makes sense, and therefore expected. Finally, Fig. 6 includes the variation of S-parameters with varactor position. As it is seen, the best way to increase the useful bandwidth of the device is to place it in the top position. In contrast, the parasitic response worsens when the varactor is positioned sideways or downward, as expected.

For the sake of discussion, the transmission response (S_{21} in magnitude) of the proposed equivalent circuit model and the one usually

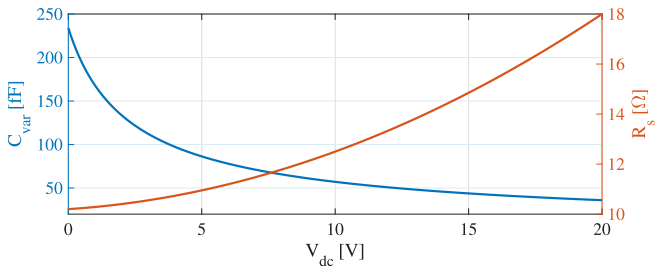

Fig. 4. Variation of the varactor capacitance (C_{var}) and resistance (R_S) with the bias voltage (V_{dc}).

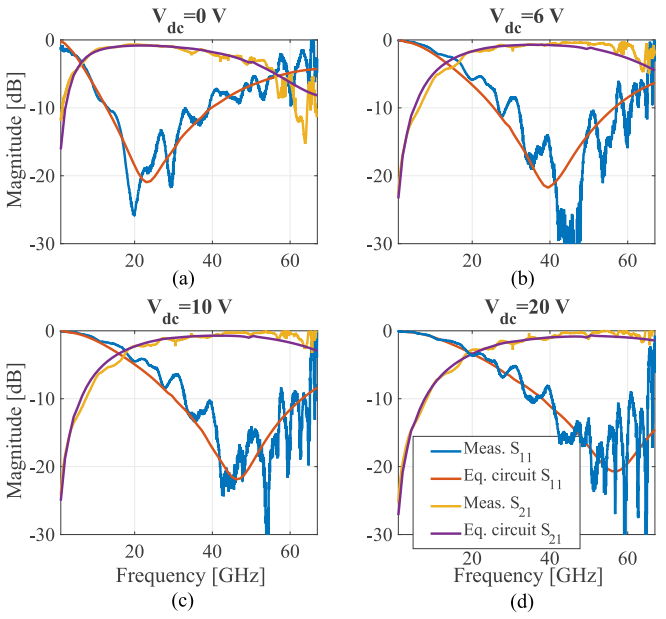

Fig. 5. Measured and equivalent circuit S-parameters of the varactor, using (a) 0 V, (b) 6 V, (c) 10 V, and (d) 20 V bias reverse voltage.

found in PIN diode and varactor datasheets (manufacturer model) are compared in Fig. 7. Concerning Fig. 7(a), related to the PIN diode, it can be seen for the two states (ON and OFF) the responses of the two compared circuit models are similar up to about 20 GHz. From this frequency, the difference between the two starts to diverge, where the proposed equivalent model captures the behavior of the measured PIN diode. Regarding Fig. 7(b), the difference between the two circuit models is more pronounced from about 30 GHz onwards. Therefore, the proposed equivalent circuit models reproduce better the PIN and varactor diode behavior in the millimeter-wave frequency band.

3.3. Phase performance of the diodes

The key point in using PIN diodes and varactors for reconfigurable device design is the range of phase variation that can be provided. Therefore, studying how the phase varies as a function of bias voltage and frequency is very convenient. Fig. 8(a) and (b) show the measured and obtained S_{21} phase value of the PIN diode and varactor in the bias point chosen in previous sections. As seen, there is an excellent agreement between the phase values along the whole measurement bandwidth. Slight deviations in low frequency are because the TRL calibration kit designed, which included only one line was not intended to cover the range below 5 GHz. This fact could be easily corrected by using a Multiline TRL kit, but the focus is high-frequency parasitics. However, what is important is the phase difference between states. In this sense, a comparison between the range of phase differences

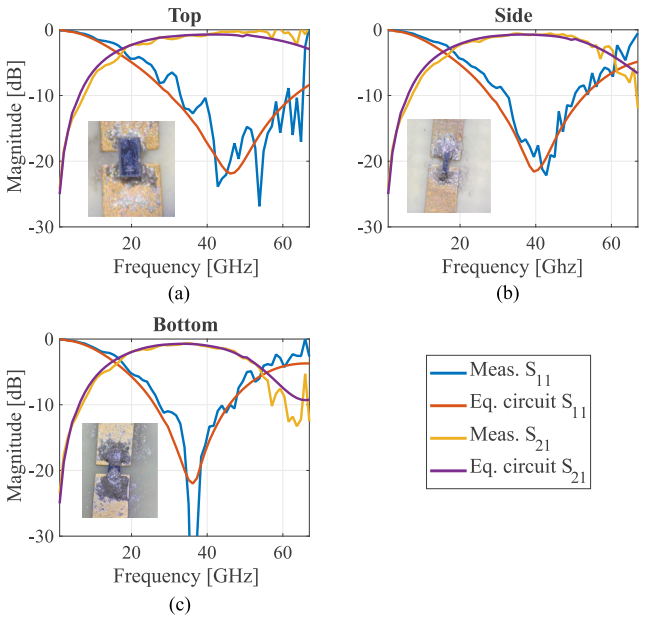

Fig. 6. Measured and equivalent circuit S-parameters of the varactor, welded in top position (a), side position (b), and bottom position (c) using V_{dc} = 10 V bias reverse voltage.

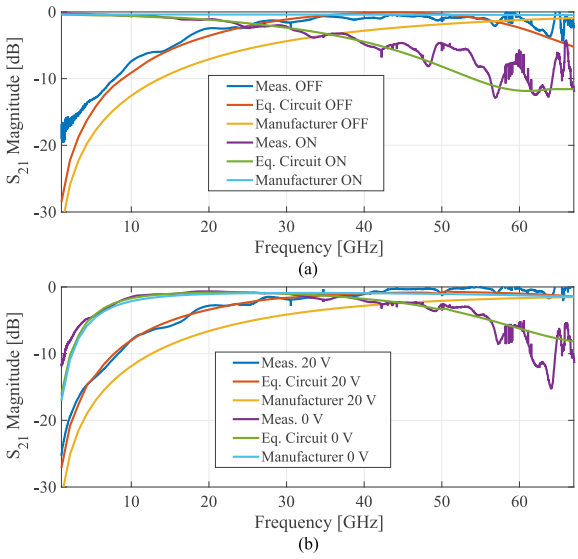

Fig. 7. Magnitude comparison between the measured S_{21}, manufacturer model S-parameter, and the equivalent circuit for (a) the PIN diode and (b) the varactor at different bias voltages.

that can be achieved with the PIN diode in OFF–ON and varactor states between 20 V and 0 V (reverse bias voltage) along the frequency is presented. Fig. 8(c) shows the comparison, including the manufacturer's equivalent circuit, i.e., without pad and gap effects. The values of the manufacturer models are computed for our intrinsic equivalent circuit. As can be seen, the PIN diode allows a broader range of phase variation than the varactor. However, the phase variation of the varactor remains flatter with frequency, a point to consider for broadband designs or in frequencies above 40 GHz. It can be seen how, at this frequency, our design clearly fits the measured parameters better than the manufacturer's model. This fact is essential since it indicates that the manufacturer's model is valid up to about 40 GHz, and the results are acceptable. However, above that frequency, it is convenient to use the equivalent model that we propose to consider

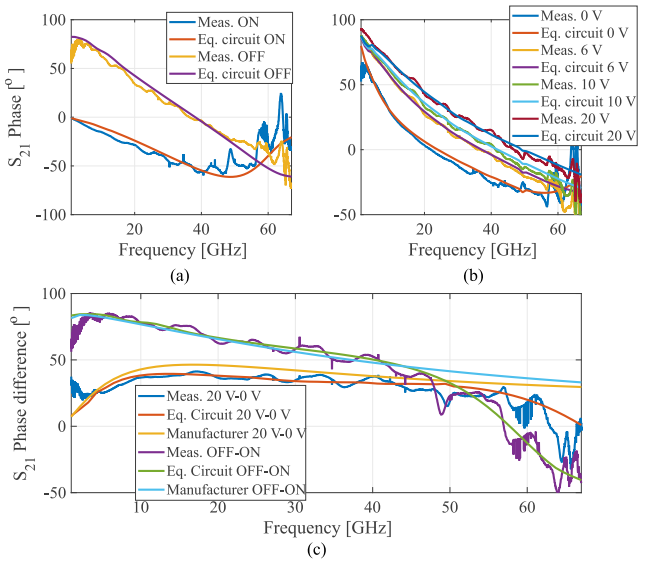

Fig. 8. Measured and equivalent circuit S_{21} phase of (a) the PIN diode and (b) the varactor. (c) Phase difference comparison with the manufacturer model S-parameter of the PIN diode and varactor at different bias voltages.

the real phase difference in the diodes studied. Despite this fact, it is important to mention that the measurements, starting at approximately 50 GHz (for PIN diode) or 55 GHz (for varactor), begin to show a significant deterioration due to unpredictable effects such as peaks and internal resonances of the device. These effects can hardly be corrected, as they are even different depending on the chip used and its position, complicating the repeatability of the experiment. On the other hand, it is also worth mentioning that the phase difference between states starts to be very small at these frequencies. This fact can be observed in the phase difference drop in Fig. 8(c).

3.4. Comparison and practical considerations

Tables 2 and 3 compare the circuit values of PIN and varactor diode, respectively, considered in some studies in the literature. Regarding Table 2, which considers the PIN model of this paper, it can be observed that most of the research works that use this diode model use the values reported in one of the first characterization studies of this PIN diode realized up to 20 GHz [17]. In contrast, the present work performs a characterization up to 67 GHz. It considers the effect of pads, which has been identified as necessary for the phase behavior at frequencies above 45 GHz [see Fig. 8]. The other part of the extrinsic model, the one related to the gap, is not included in the equivalent circuit but is introduced in the electromagnetic simulator by entering the dimensions of the corresponding gap.

Regarding the comparison with the research works that use the same varactor model, we note that no complete characterization of this varactor has been done. Previously, some studies using this varactor model consider only the parasitic resistance and the capacity range C_{var}, the only information found in their datasheet [25]. In other studies, they complete the effects of the varactor circuit model by including the physical model in the electromagnetic simulator as applied in [21]. In this way, the effect of the pads is also considered, taking into account their impact for frequencies higher than 50 GHz. Therefore, to obtain accurate results of the diode behavior at frequencies higher than 40 GHz, it is essential to include either the corresponding S-parameters (through the equivalent circuits) or the complete physical model of the diode to consider the parasitic effects. However, this information about the internal elements/geometries of the diodes is not always available.

The research works in comparative Tables 2 and 3 show antenna designs where the PIN diode or varactor is employed to reconfigure the radiated beam electronically. Modifying the main beam direction is mainly due to the change of the relative phase shift between the elements forming the antenna array. The maximum operating frequency found in these antenna designs is 32 GHz. For a reconfigurable antenna design with a higher operating frequency, it would be more accurate to use the proposed equivalent circuit models for PIN diodes and varactors, as these would capture the phase behavior provided by these diodes up to 67 GHz. Consequently, the electromagnetic simulation at the design stage is more accurate, and the expected behavior of the fabricated prototype is more predictable.

Table 2
Comparison with the research works where the equivalent circuits of the PIN diode MA4AGP907 are extracted or used.

Ref.	Freq. (GHz)	R_{on} | R_{off} (Ω) | (kΩ)	L_s (pH)	C_{off} (fF)	Pads consideration
[13]	9–10	4.2 | 300	50	42	No
[14]	10.1	4.2 | 300	50	50	No
[15]	27–29	4.2 | 300	50	42	No
[16]	0.1–20	3.5 | 200	55	27	No
[17]	1–20	3.6 | 300	50	42	No
[18]	26–31	4.2 | 300	50	42	No
This work	1–67	3.4 | 100	30.3	41.3	Yes

Table 3
Comparison with the research works where the equivalent circuits of the varactor MAVR-011020-1411 are extracted or used.

Ref.	Freq. (GHz)	R_s (Ω)	L_s (pH)	C_{par} (fF)	Pads consideration
[19]	27–30	13.2	n. a.	n. a.	No
[20]	10.65	13.2	n. a.	n. a.	No
[21]	22–32	8	n. a.[a]	n. a.[a]	Yes[a]
[22]	29–31	7	n. a.	n. a.	No
[23]	15–26	7.5	n. a.	10	Yes[a]
This work	1–67	10.2[b]	88.5	9	Yes

[a] It is taken into account in the electromagnetic software by introducing the physical diode model.
[b] It depends on the bias voltage [see Eq. (5)].

4. Conclusion

In this work, we have proposed a broadband parasitic model for PIN diodes and varactors up to 67 GHz. For this purpose, the diodes were mounted on a microstrip line, and their responses were measured at different bias points and soldering positions. Subsequently, a model with several parasitic effects, including the gap and pads, has been modeled and optimized to ensure that its frequency response is similar to that of the measured varactor. Finally, it has been verified that there is an excellent agreement between the measurements and the response of the equivalent circuit models proposed, showing that the useful bandwidth can reach up to approximately 55 GHz. In contrast, the PIN diode is up to about 50 GHz. This modeling has not been reported yet, and it will be helpful to perform more accurate designs using these diode models and properly know their frequency limits since the manufacturer does not provide this information.

CRediT authorship contribution statement

Mario Pérez-Escribano: Writing – original draft, Validation, Methodology, Investigation, Conceptualization. **Ángel Palomares-Caballero:** Writing – original draft, Validation, Supervision, Methodology, Investigation, Conceptualization. **Pablo Padilla:** Validation, Supervision, Project administration, Methodology, Investigation, Funding acquisition, Conceptualization. **Juan F. Valenzuela-Valdés:** Validation, Supervision, Project administration, Methodology, Investigation, Funding acquisition, Conceptualization. **Enrique Márquez-Segura:** Formal analysis, Writing – review & editing.

Declaration of competing interest

The authors declare the following financial interests/personal relationships which may be considered as potential competing interests: Mario Perez-Escribano reports financial support was provided by Government of Spain Ministry of Universities. Pablo Padilla reports financial support was provided by Spain Ministry of Science and Innovation. Juan F. Valenzuela-Valdes reports financial support was provided by Spain Ministry of Science and Innovation. If there are other authors, they declare that they have no known competing financial interests or personal relationships that could have appeared to influence the work reported in this paper.

Data availability

No data was used for the research described in the article.

Acknowledgments

This work has been supported by grant PID2020-112545RB-C54 funded by MCIN/AEI/10.13039/501100011033 and by the European Union NextGenerationEU/PRTR. It has also been supported by grants PDC2022-133900-I00, TED2021-129938B-I00, TED2021-131699B-I00, by Contract SAD 22006912 (SuMeRIO) of Brittany Region and by Ministerio de Universidades and the European Union NextGenerationEU, under Programa Margarita Salas. Funding for open access charge: Universidad de Málaga / CBUA.

References

[1] Lee J, Tejedor E, Ranta-aho K, Wang H, Lee K-T, Semaan E, Mohyeldin E, Song J, Bergljung C, Jung S. Spectrum for 5G: Global status, challenges, and enabling technologies. IEEE Commun Mag 2018;56(3):12–8. http://dx.doi.org/10.1109/MCOM.2018.1700818.

[2] Rangan S, Rappaport TS, Erkip E. Millimeter-wave cellular wireless networks: Potentials and challenges. Proc IEEE 2014;102(3):366–85. http://dx.doi.org/10.1109/JPROC.2014.2299397.

[3] Pablo Zapata Cano H, Zaharis ZD, Yioultsis TV, Kantartzis NV, Lazaridis PI. Pattern reconfigurable antennas at millimeter-wave frequencies: A comprehensive survey. IEEE Access 2022;10:83029–42. http://dx.doi.org/10.1109/ACCESS.2022.3196456.

[4] Ojaroudi Parchin N, Jahanbakhsh Basherlou H, Al-Yasir YIA, M. Abdulkhaleq A, A. Abd-Alhameed R. Reconfigurable antennas: Switching techniques—A survey. Electronics 2020;9(2). http://dx.doi.org/10.3390/electronics9020336.

[5] Costantine J, Tawk Y, Barbin SE, Christodoulou CG. Reconfigurable antennas: Design and applications. Proc IEEE 2015;103(3):424–37. http://dx.doi.org/10.1109/JPROC.2015.2396000.

[6] Shah I, Hayat S, Basir A, Zada M, Shah S, Ullah S, Ullah S. Design and analysis of a hexa-band frequency reconfigurable antenna for wireless communication. AEU - Int J Electron Commun 2019;98:80–8. http://dx.doi.org/10.1016/j.aeue.2018.10.012.

[7] Singh A, Dubey R, Jatav R, Meshram MK. Electronically reconfigurable microstrip antenna with steerable beams. AEU - Int J Electron Commun 2022;149:154179. http://dx.doi.org/10.1016/j.aeue.2022.154179.

[8] Kumar J, Basu B, Talukdar FA, Nandi A. Stable-multiband frequency reconfigurable antenna with improved radiation efficiency and increased number of multiband operations. IET Microw Antennas Propag 2019;13(5):642–8. http://dx.doi.org/10.1049/iet-map.2018.5602.

[9] Chaouche YB, Bouttout F, Nedil M, Messaoudene I, Mabrouk IB. A frequency reconfigurable U-shaped antenna for dual-band WIMAX/WLAN systems. Prog Electromagn Res C 2018;87:63–71. http://dx.doi.org/10.2528/PIERC18071004.

[10] Trichopoulos GC, Theofanopoulos P, Kashyap B, Shekhawat A, Modi A, Osman T, Kumar S, Sengar A, Chang A, Alkhateeb A. Design and evaluation of reconfigurable intelligent surfaces in real-world environment. IEEE Open J Commun Soc 2022;3:462–74. http://dx.doi.org/10.1109/OJCOMS.2022.3158310.

[11] Alex-Amor A, Moreno-Núñez J, Fernández-González JM, Padilla P, Esteban J. Parasitics impact on the performance of rectifier circuits in sensing RF energy harvesting. Sensors 2019;19(22). http://dx.doi.org/10.3390/s19224939, URL https://www.mdpi.com/1424-8220/19/22/4939.

[12] Singh A, Mandal MK. Parasitic compensation and hence isolation improvement of PIN diode-based switches. IEEE Trans Circuits Syst II 2021;68(1):97–101. http://dx.doi.org/10.1109/TCSII.2020.3000587.

[13] Wu F, Lu R, Wang J, Jiang ZH, Hong W, Luk K-M. A circularly polarized 1 bit electronically reconfigurable reflectarray based on electromagnetic element rotation. IEEE Trans Antennas and Propagation 2021;69(9):5585–95. http://dx.doi.org/10.1109/TAP.2021.3069551.

[14] Nam Y-H, Kim Y, Lee S-G, Lee J-H. Hybrid reflectarray antenna of passive and active unit cells for highly directive two-direction beam steering. IEEE Access 2023;11:6299–304. http://dx.doi.org/10.1109/ACCESS.2022.3232120.

[15] Wan X, Xiao Q, Zhang YZ, Li Y, Eisenbeis J, Wang JW, Huang ZA, Liu HX, Zwick T, Cui TJ. Reconfigurable sum and difference beams based on a binary programmable metasurface. IEEE Antennas Wirel Propag Lett 2021;20(3):381–5. http://dx.doi.org/10.1109/LAWP.2021.3050808.

[16] Wang X, Qin P-Y, Tuyen Le A, Zhang H, Jin R, Guo YJ. Beam scanning transmitarray employing reconfigurable dual-layer huygens element. IEEE Trans Antennas and Propagation 2022;70(9):7491–500. http://dx.doi.org/10.1109/TAP.2022.3176857.

[17] Clemente A, Dussopt L, Sauleau R, Potier P, Pouliguen P. 1-bit reconfigurable unit cell based on PIN diodes for transmit-array applications in X -band. IEEE Trans Antennas and Propagation 2012;60(5):2260–9. http://dx.doi.org/10.1109/TAP.2012.2189716.

[18] Clemente A, Diaby F, Palma LD, Dussopt L, Sauleau R. Experimental validation of a 2-bit reconfigurable unit-cell for transmitarrays at ka-band. IEEE Access 2020;8:114991–7. http://dx.doi.org/10.1109/ACCESS.2020.3003698.

[19] Javanbakht N, Amaya RE, Shaker J, Syrett B. Fixed frequency beam-scanning HMSIW-based leaky-wave antenna composed of circular slots in V-Shape configuration. IEEE Access 2021;9:52891–901. http://dx.doi.org/10.1109/ACCESS.2021.3070195.

[20] Teodorani L, Vernì F, Giordanengo G, Gaffoglio R, Vecchi G. Experimental demonstration of beam scanning of dual-metasurface antenna. Electronics 2023;12(8). http://dx.doi.org/10.3390/electronics12081833, URL https://www.mdpi.com/2079-9292/12/8/1833.

[21] Chen Q, Ala-Laurinaho J, Khripkov A, Ilvonen J, Moreno RM, Viikari V. Varactor-based frequency-reconfigurable dual-polarized mm-wave antenna array for mobile devices. IEEE Trans Antennas and Propagation 2023;71(8):6628–38. http://dx.doi.org/10.1109/TAP.2023.3287679.

[22] Cho S, Youn Y, Hong W, Song H-J. Reconfigurable binary-amplitude fresnel zone plate for millimeter-wave beamforming. IEEE Trans Antennas and Propagation 2021;69(10):6444–52. http://dx.doi.org/10.1109/TAP.2021.3070072.

[23] Rotshild D, Abramovich A. Realization and validation of continuous tunable metasurface for high resolution beam steering reflector at K-band frequency. Int J RF Microw Comput-Aided Eng 2021;31(4):e22559. http://dx.doi.org/10.1002/mmce.22559, arXiv:https://onlinelibrary.wiley.com/doi/pdf/10.1002/mmce.22559 URL https://onlinelibrary.wiley.com/doi/abs/10.1002/mmce.22559.

[24] MA-COM technology solutions, MA4agp907 GaAs flip-chip PIN diode. 2024, https://cdn.macom.com/datasheets/MA4AGP907_MA4AGFCP910.pdf.

[25] MA-COM technology solutions, MAVR-011020-1411 GaAs flip-chip varactor diode. 2024, https://cdn.macom.com/datasheets/MAVR-011020-1141.pdf.

[26] Rorsman N, Garcia M, Karlsson C, Zirath H. Accurate small-signal modeling of HFET's for millimeter-wave applications. IEEE Trans Microw Theory Tech 1996;44(3):432–7. http://dx.doi.org/10.1109/22.486152.

[27] Tang AY, Drakinskiy V, Yhland K, Stenarson J, Bryllert T, Stake J. Analytical extraction of a schottky diode model from broadband S-parameters. IEEE Trans Microw Theory Tech 2013;61(5):1870–8. http://dx.doi.org/10.1109/TMTT.2013.2251655.

[28] Sievert B, Degen M, Svejda JT, Erni D, Rennings A. An analytical model to approximate the radiation conductance of microstrip gaps. In: 2022 52nd European microwave conference (euMC). 2022, p. 238–41. http://dx.doi.org/10.23919/EuMC54642.2022.9924365.

[29] Deschrijver D, Mrozowski M, Dhaene T, De Zutter D. Macromodeling of multiport systems using a fast implementation of the vector fitting method. IEEE Microw Wirel Compon Lett 2008;18(6):383–5. http://dx.doi.org/10.1109/LMWC.2008.922585.